Multistep effect in $^{16}O + ^{16}O$ inelastic scattering

M. Takashina[1,*] and Y. Sakuragi[2,3]
[1]*Research Center for Nuclear Physics (RCNP), Osaka University, Ibaraki, Osaka 567-0047, Japan*
[2]*Department of Physics, Osaka City University, Osaka 558-8585, Japan*
[3]*RIKEN Nishina Center, Hirosawa 2-1, Wako, Saitama 351-0198, Japan*
(Received 9 June 2009; published 9 July 2009)

We have analyzed $^{16}O + ^{16}O$ inelastic scattering to the single 2^+_1 and 3^-_1 channels at incident energies of $E_{lab} = 350$ and 1120 MeV by a microscopic coupled-channel calculation. We have found that the strong rotational coupling among the channels of the $\alpha + ^{12}C_{g.s.}$ type cluster states plays an important role in reproducing the angular distribution of the 2^+_1 channel for both energies. We have also found that the coupling with the 0^+_2, 2^+_1, and 4^+_1 channels as well as those among the shell channels has a large effect on the 3^-_1 channel cross sections at $E_{lab} =$ 350 MeV. However, their absolute values could not be reproduced by our calculation, unless we assumed that the strengths of the $3^-_1 \to 0^+_2, 2^+_1, 4^+_1$ transitions were unphysically strong.

DOI: 10.1103/PhysRevC.80.014605 PACS number(s): 25.55.Ci, 24.10.Eq, 27.20.+n

I. INTRODUCTION

The double folding model (DFM) is known to be a useful tool for obtaining the internucleus potential. Indeed, DFM analyses using density-dependent-type nucleon-nucleon potentials, such as the DDM3Y [1] and CDM3Y6 [2], with a phenomenological imaginary potential have successfully reproduced the nuclear rainbow phenomena observed in $^{16}O + ^{16}O$ elastic scattering [3,4]. Since the nuclear rainbow pattern in the angular distribution is sensitive to the shape and depth of the real part of the optical potential, these results indicate that the DFM gives a precise real optical potential.

Because of these successful results for elastic scattering, it is natural to expect that the coupled-channel (CC) or DWBA calculation based on the DFM can also precisely reproduce the $^{16}O + ^{16}O$ inelastic angular distribution. However, it was shown in Refs. [4,5] that the magnitude of the inelastic scattering cross section to the single excitation channels of the 2^+_1 ($E_x = 6.92$ MeV) and 3^-_1 (6.13 MeV) states could not be reproduced by DFM analyses simultaneously with the elastic angular distribution. The calculation gives order-of-magnitude larger cross sections than the experimental data, as long as the imaginary potential of the inelastic channels is assumed to be the same as that of the elastic one (and the coupling potential is complex), even though the transition densities used gave the correct electric transition strengths $B(E2)$ and $B(E3)$.

In Ref. [5], the authors pointed out that one needed to artificially increase the imaginary-potential strength to reproduce the absolute values of the experimental cross sections for these channels. This may suggest that a large portion of flux induced in these inelastic channels from the elastic channel may have leaked out into other reaction channels, which must be strongly connected to these inelastic channels. In fact, the calculation of Ref. [5] included only the ground, 2^+_1 and 3^-_1 states. The validity of this limited model space can be justified only when the coupling with other channels is sufficiently weak.

It is well known [6] that the 2^+_1 state in ^{16}O is a member of the rotational band consisting of the 0^+_2 (6.05 MeV), 2^+_1, and 4^+_1 (10.36 MeV) states (with the 0^+_2 state being the bandhead), which have a well-developed $\alpha + ^{12}C_{g.s.}$ type cluster structure, and the intraband transitions among the states are very strong. Therefore, it is expected that coupling with the 0^+_2 and 4^+_1 channels has a large effect on the inelastic cross section in the 2^+_1 channel. Furthermore, 1^-_2 (9.59 MeV), 3^-_2 (11.60 MeV), and 5^-_1 (14.68 MeV) states are known to form a negative-parity rotational band, which is interpreted to be the inversion doublet [7] of the positive-parity rotational band with 0^+_2, 2^+_1, and 4^+_1 states and, hence, the couplings among the states belonging to the positive-parity band and those to the negative-parity bands are also expected to be important. Similarly, since the 3^-_1 state has a shell-model-like structure, the coupling with the channels including other low-lying shell states as well as the ground state may be important. Indeed, in the CC analysis of Ref. [4], the 1^-_1 and mutual-3^-_1 channels are included, although the resultant cross sections of the 3^-_1 channel still overestimates the experimental data, as already mentioned. Another candidate would be the 2^-_1 (8.87-MeV) state, which also has a shell-model-like structure [6] and is expected to have a non-negligible transition strength to the 3^-_1 state.

In this paper, we investigate the multistep effect on the 2^+_1 and 3^-_1 single excitation channels of $^{16}O + ^{16}O$ inelastic scattering by the CC calculation including the single excitation channels of all the states in ^{16}O below the excitation energy $E_x = 10.5$ MeV and the 3^-_2 and 5^-_1 states, and we discuss the possibility of resolving the overestimation problem of the 2^+_1 and 3^-_1 channel cross sections.

II. FORMALISM

A. Microscopic coupled-channel method

In the present study, we perform microscopic coupled-channel (MCC) calculations, where the real parts of the diagonal and coupling potentials are given by the DFM:

$$V_{\alpha(ij),\beta(k\ell)}(\mathbf{R}) = \int \rho^{(a)}_{ik}(\mathbf{r}_a)\rho^{(A)}_{j\ell}(\mathbf{r}_A) \times v_{NN}(\mathbf{r}_a + \mathbf{R} - \mathbf{r}_A)d\mathbf{r}_a d\mathbf{r}_A, \quad (1)$$

*takasina@rcnp.osaka-u.ac.jp

where $\rho^{(a)}_{ik}(\rho^{(A)}_{j\ell})$ represents the transition density of the projectile (target) nucleus between the state $i(j)$ in channel α and the state $k(\ell)$ in channel β. For v_{NN}, we adopt the DDM3Y interaction [1] with the zero-range exchange term. To reproduce the elastic data precisely, we will introduce the normalization factor close to the unity for the real folded potential.

Because DDM3Y has no imaginary part, we add the imaginary potential, for which we consider the following two assumptions:

(i) The shape of the imaginary potential is the same as that of the real potential for all the diagonal and coupling terms. Then, the generalized optical potential is written as

$$U_{\alpha,\beta}(\mathbf{R}) = (N_R + \imath N_I)V_{\alpha,\beta}(\mathbf{R}), \tag{2}$$

where N_R and N_I are the normalization factor for the real and imaginary parts, respectively, and are determined so as to reproduce the elastic angular distribution. N_R is restricted to be close to unity as previously mentioned.

(ii) The diagonal part of the imaginary potential is assumed to be of Woods-Saxon shape;

$$W_{\text{diag.}}(R) = -W_0\left[1 + \exp\left(\frac{R - R_W}{a_W}\right)\right]^{-1}. \tag{3}$$

The parameters W_0, R_W, and a_W are determined so as to reproduce the elastic angular distribution and are taken to be common to all the channels. In this case, the real folded potential is again multiplied by the normalization factor N_R, and its value is determined simultaneously with the Woods-Saxon imaginary parameters. Since the coupling potential would be complex, we assume the deformed optical potential model type form factor [5]

$$W^{(\gamma)}_{\text{coupl.}}(R) = -\delta_\gamma \frac{dW_{\text{diag.}}(R)}{dR} \tag{4}$$

for the coupling term of the imaginary potential. In Eq. (4), γ represents the pair of the channels and δ_γ is the deformation length of the corresponding transition. In the analysis of the inelastic scattering to the 2^+_1 and 3^-_1 channels, the values of $\delta_{2^+_1\to\text{g.s.}}$ and $\delta_{3^-_1\to\text{g.s.}}$ are important. We take them from Ref. [5]: $\delta_{2^+_1\to\text{g.s.}} = 1.038$ fm and $\delta_{3^-_1\to\text{g.s.}} = 1.825$ fm. However, we assume that $\delta_\gamma = 0$ for the other transitions to avoid the ambiguity from the choice of the deformation length. This assumption would be justified because the coupling terms other than the $^{16}\text{O}_{\text{g.s.}} + {}^{16}\text{O}_{\text{g.s.}} \to {}^{16}\text{O}_{\text{g.s.}} + {}^{16}\text{O}(2^+_1, 3^-_1)$ transitions have just an indirect effect on the 2^+_1 and 3^-_1 channels as the distortion.

It should be noted that no adjustable parameters for the 2^+_1 and 3^-_1 channels are included in either (I) or (II).

The coupled-channel equations are solved by the Stormer method with the mesh $\Delta R = 0.01$ fm, and the matching radius is $R_{\max} = 15.0$ fm. We include the partial waves up to $J_{\max} = 150$ for $E_{\text{lab}} = 350$ MeV and $J_{\max} = 250$ for $E_{\text{lab}} = 1120$ MeV.

TABLE I. The states of ^{16}O included in the present calculation classified into the shell-model type, $\alpha + {}^{12}\text{C}_{\text{g.s.}}$ type, and $\alpha + {}^{12}\text{C}(2^+_1)$ type structures based on the results in Ref. [6] (see also the text). The excitation energies (in MeV) are also given in parentheses.

Shell model SH	$\alpha + {}^{12}\text{C}_{\text{g.s.}}$		$\alpha + {}^{12}\text{C}_{\text{g.s.}}(2^+_1)$ CL-C
	CL-A	CL-B	
$0^+_1(0.0)$	$0^+_2(6.05)$	$1^-_2(9.59)$	$2^+_2(9.84)$
$3^-_1(6.13)$	$2^+_1(6.92)$	$3^-_2(11.60)$	
$1^-_1(7.12)$	$4^+_1(10.36)$	$5^-_1(14.68)$	
$2^-_1(8.87)$			

B. States of ^{16}O

In addition to the ground, 2^+_1 and 3^-_1 states, we consider the 1^-_1, 2^-_1, 0^+_2, 4^+_1, 1^-_2, 3^-_2, 5^-_1, and 2^+_2 states in ^{16}O as mentioned in the introduction. Their structure type (shell-model type or $\alpha + {}^{12}\text{C}$ cluster type) and the excitation energies are summarized in Table I. For the later analysis, we classify the states into four groups according to the results described in Ref. [6]. The 0^+_2, 2^+_1, and 4^+_1 states in ^{16}O form the rotational band with an $\alpha + {}^{12}\text{C}_{\text{g.s.}}$ type cluster structure, and the 1^-_2, 3^-_2, and 5^-_1 states are the inversion doublet of them. Hence, we refer to the former three states as CL-A and to the latter three states as CL-B. The 2^+_2 state has an $\alpha + {}^{12}\text{C}(2^+_1)$ type structure and is referred to as CL-C. The ground, 3^-_1, 1^-_1, and 2^-_1 states are usually called the shell-model-like states (SH), because their main configurations are the Pauli allowed states with the minimum number of oscillator quanta in the shell model.

For the diagonal and transition densities of the ground, 2^+_1, 3^-_1, 1^-_1, 0^+_2, and 2^+_2 states, we use the ones obtained by the $\alpha + {}^{12}\text{C}$ orthogonality-condition-model (OCM) calculation [8] with some modifications: The transition density between the ground and $2^+_1(3^-_1)$ states is normalized so as to reproduce the experimental electric transition strength $B(E2)[B(E3)]$. We also normalize the transition density between 0^+_2 and 2^+_1 states to give the correct $B(E2)$ value. Since some transition densities are not available in the OCM calculation, we add the missing transition densities that are expected to be important with several assumptions. We assume that the transition density between the 3^-_1 and 1^-_1 states can be represented by a derivative form of the average of the diagonal densities of the 3^-_1 and 1^-_1 states, whose strength is adjusted with the deformation length to reproduce the electric transition strength as done in Ref. [4]. The $\lambda = 1$ components (where λ represents the multipolarity) of the transition densities from the 3^-_1 state to the CL-A and CL-C states are assumed to be the same as that between the ground and 1^-_1 states. Transition density strengths that are too large might have been assigned in the present prescription than what we expect from the actual $3^-_1 \to$ CL-A, CL-C strengths. However, since no experimental information

for these transition strengths are so far available, we adopt the prescription mentioned here for these transitions. The $\lambda = 3$ components are made in the same manner as the $1^-_1 \to 3^-_1$ case with the deformation lengths determined in the following assumption: These transitions are the ones between the cluster states and the shell-model-like state (referred to as the *cluster-shell transition*). When we see the electric transition strengths of the other cluster-shell transitions, namely $2^+_1, 4^+_1 \to$ g.s., we find that their experimental values $B(E2)$ and $B(E4)$ are 3–4 Weisskopf units (W.u.) [9]. Therefore, we assume that $B(E3)$ values of the CL-A, CL-C $\to 3^-_1$ transitions are $B(E3) = 3.5$ W.u. for all the cases, and the deformation lengths are determined so as to give this value.

The 4^+_1, 1^-_2, 3^-_2, and 5^-_1 states are known to have the $\alpha + {}^{12}\mathrm{C}_{\mathrm{g.s.}}$ type cluster structure [6] and are expected to have an important effect on the 2^+_1 channel. Therefore, we calculate the transition densities from these states to the 0^+_2 and 2^+_1 states as well as their diagonal densities in the following procedure. We assume that the relative wave function between α and $^{12}\mathrm{C}_{\mathrm{g.s.}}$ can be obtained by a simple potential model calculation, namely the separation energy method, in which the potential geometry is assumed to be of Woods-Saxon type with a range parameter $R_0 = 1.25 \times 12^{1/3}$ fm and a diffuseness parameter $a_0 = 0.65$ fm. The depth of the potential is adjusted to reproduce the separation energy for the bound state and the resonance energy for the unbound state, with the appropriate oscillator quantum number of the intercluster motion for each state assumed to take account of the Pauli principle between the α and $^{12}\mathrm{C}_{\mathrm{g.s.}}$ clusters. For the resonance state, we use the momentum-bin prescription in the continuum-discretized coupled-channel (CDCC) method [10] to make a wave packet. Using the obtained relative wave function $\psi_{IM}(\mathbf{r}')$, we can write the diagonal or transition density as

$$\rho^{(^{16}\mathrm{O})}_{IM,I'M'}(\mathbf{r}) = \langle \psi_{IM}(\mathbf{r}') | \rho^{(\alpha)}_0\left(\mathbf{r} + \tfrac{3}{4}\mathbf{r}'\right) + \rho^{(^{12}\mathrm{C})}_0\left(\mathbf{r} - \tfrac{1}{4}\mathbf{r}'\right) | \psi_{I'M'}(\mathbf{r}') \rangle_{\mathbf{r}'}, \quad (5)$$

where $\mathbf{r}'$ represents the relative coordinate between α and $^{12}\mathrm{C}_{\mathrm{g.s.}}$, and I and M (I' and M') are the relative angular momentum and its z-component of the final (initial) state. In Eq. (5), $\rho^{(\alpha)}_0$ and $\rho^{(^{12}\mathrm{C})}_0$ are the ground-state densities of the α particle and ^{12}C. We normalize the transition densities made by this potential model so as to reproduce the experimental data when the corresponding transition strength is experimentally available.

The transitions between the 3^-_1 state and the CL-B states are again the cluster-shell transitions with $\lambda = 2$. Therefore, we assume that the transition densities between them are the same as that for $2^+_1 \to$ g.s. without renormalization.

The 2^-_1 state is known to have a shell-model-like structure [6]. Hence, we assume that the diagonal density of 2^-_1 is the same as that of 3^-_1 and that the transition density for $2^-_1 \to 3^-_1$ can be obtained by the same manner as the $1^-_1 \to 3^-_1$ case.

In the CC calculation, we consider the elastic channel, the single excitation channels of all the states listed in Table I, and the mutual excitation channel of 3^-_1. We call the single excitation channel of 2^+_1 the 2^+_1 channel, and similarly for the other case; the mutual excitation channel of 3^-_1 is called the mutual-3^-_1 channel.

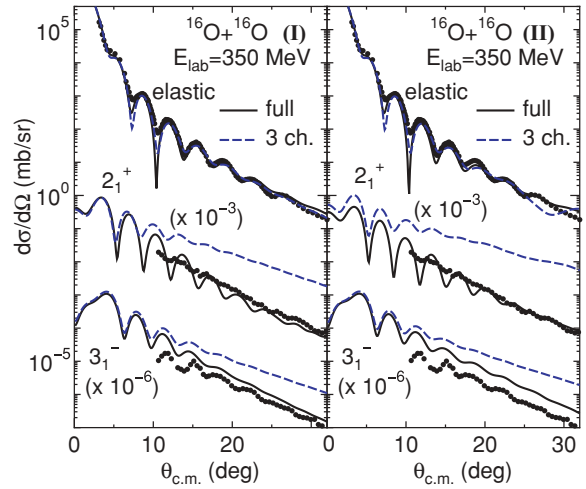

FIG. 1. (Color online) The angular distributions for the ^{16}O + ^{16}O elastic, 2^+_1 and 3^-_1 channels at an incident energy of $E_{\mathrm{lab}} =$ 350 MeV. The solid circles are the experimental data [5]. The solid curves represent the results of the full CC calculations, and the dashed curves represent the results of the three-channel calculations. The left and right panels show the results with imaginary potentials (I) and (II), respectively.

III. RESULTS

The left and right panels of Fig. 1 show the results of the CC calculations with imaginary potentials (I) and (II), respectively, at an incident energy of $E_{\mathrm{lab}} = 350$ MeV. The solid curves are for the full CC calculation, and the dashed curves are for the three-channel calculation where only the elastic, 2^+_1 and 3^-_1 channels are included. The normalization factor N_R and the imaginary potential parameters are determined so as to reproduce the elastic angular distribution in each calculation separately, and their values are listed in Table II. It is found that the result of the three-channel calculation largely overestimates the experimental cross sections of both the 2^+_1 and 3^-_1 channels, which is consistent with the results in Refs. [4,5]. However, when we include the coupling with the other channels, the calculated cross sections (solid curve) are reduced and excellently reproduce the absolute value of the experimental data for the 2^+_1 channel in both (I) and (II).

TABLE II. The parameter values obtained by the optimum fits with the CC calculations.

E_{lab} (MeV)		(I)		(II)			
		N_R	N_I	N_R	W_0 (MeV)	R_W (fm)	a_W (fm)
350	full	1.1	0.45	1.1	27.0	5.4	0.73
	3 ch.	1.1	0.35	1.1	17.0	5.4	0.73
1120	full	1.176	0.6	1.1	26.0	5.4	0.787
	3 ch.	1.176	0.6	1.1	26.0	5.4	0.787

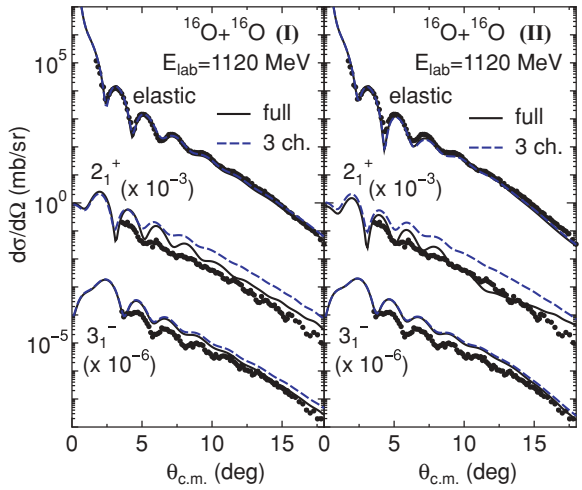

FIG. 2. (Color online) Same as Fig. 1, but for $E_{\rm lab} = 1120$ MeV.

The 3_1^- channel cross sections of the full-channel calculation in (I) are also found to be largely improved compared with the three-channel case, although they still slightly overestimate the experimental values. In calculation (II), the multistep effect on the 3_1^- channel is visible, but it is not sufficient to reproduce the experimental data.

We also perform the same calculations for $E_{\rm lab} = 1120$ MeV, for which one might think that the multistep coupling effect is negligible. The results are shown in Fig. 2. In spite of the high incident energy, the multistep coupling effect is considerable for the 2_1^+ channel in both (I) and (II) because of the strong multistep coupling effect as is the case for $E_{\rm lab} = 350$ MeV. Calculation (II) reproduces the experimental cross sections of this channel fairly well, whereas calculation (I) slightly overestimates. For the 3_1^- channel, the coupling effect is visible in calculation (I), but it is negligible in calculation (II). This means that the estimation of the multistep effect on the 3_1^- channel in (II) is weaker than that in (I), and this tendency has also been seen in the $E_{\rm lab} = 350$ MeV case shown in Fig. 1.

To investigate the reaction mechanism, we analyze these results for $E_{\rm lab} = 350$ MeV with imaginary potential (I) by performing various types of CC calculations. In the following calculations, we use the imaginary potential parameter $N_I = 0.45$, which was obtained in the full channel calculation. The coupling scheme that will be considered in the following is summarized in Table III.

TABLE III. Excited channels included in the CC calculations. CL-A, CL-B, CL-C, and SH represent the group of states (see Table I). The states are for the single excitation channels, except for the mutual-3_1^- one. In this table, SH includes the mutual-3_1^- channel.

Case 1 = 2_1^+
Case 2 = CL-A
Case 3 = CL-A + CL-B + CL-C
Case 4 = 3_1^-
Case 5 = SH
Case 6 = CL-A + SH
Full = CL-A + CL-B + CL-C + SH

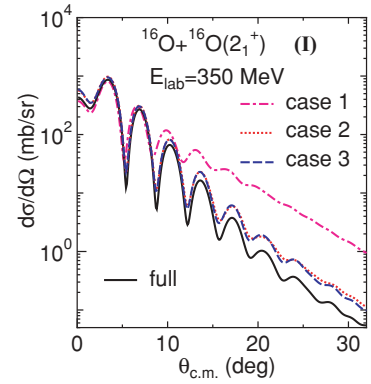

FIG. 3. (Color online) Angular distributions of the 2_1^+ channel at an incident energy of $E_{\rm lab} = 350$ MeV by the CC calculations with the coupling scheme of cases 1–3 (see Table III) as well as the full channel calculation using imaginary potential (I).

We first see the 2_1^+ channel. The dot-dashed curve in Fig. 3 represents the CC calculation where only the elastic and 2_1^+ channels are included (case 1), and it is found to largely overestimate the full CC result (solid). However, when we include the coupling with the CL-A channels (case 2, dotted), the cross sections in the backward angles are drastically reduced and are close to the solid curve. Therefore, it can be said that the coupling effect on the 2_1^+ channel is almost exhausted by the 0_2^+ and 4_1^+ channels. Since the small difference is seen between the dotted and solid curves, we further add the other cluster channels, CL-B and CL-C (case 3). The result is shown by the dashed curve, and it is found that the coupling effect by the CL-B and CL-C channels is negligible. This result implies that the remaining SH channels also have a non-negligible effect on the 2_1^+ channel.

We also investigate the coupling effect on the 3_1^- channel. The dot-dashed curve in Fig. 4 represents the result of a two-channel calculation including only the elastic and 3_1^- channels (case 4). We first add the other shell channels (case 5). The dotted curve is the result of case 5, the model space of which is larger than the CC calculation of Ref. [4]. It is found that the

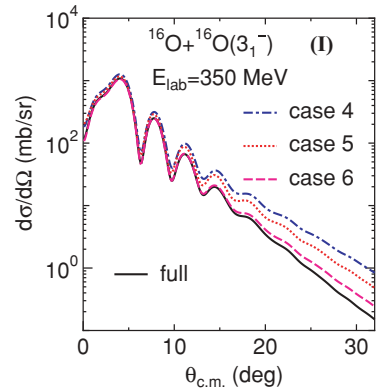

FIG. 4. (Color online) Angular distributions of the 3_1^- channel at an incident energy of $E_{\rm lab} = 350$ MeV by the CC calculations with the coupling scheme of cases 4–6 (see Table III) as well as the full channel calculation using imaginary potential (I).

coupling effect by the SH channels is smaller than expected, and the dotted curve still disagrees with the result of the full channel calculation. This result indicates that the coupling effect on the 3^-_1 channel is not exhausted by the SH channels. Hence, we further add the CL-A channels (case 6), and the result is shown by the dashed curve. It is found that the dashed curve is close to the full channel calculation and that the effect of the coupling with the CL-A channels for the 3^-_1 channel is comparable with that with the SH channels, although the 3^-_1 state has a shell-model-like structure. The small difference between the dashed and solid curves is due to the effect of the remaining CL-B and CL-C channels.

The result of this analysis indicates that the coupling between the 3^-_1 channel and the CL-A channels plays an important role in reducing the 3^-_1 channel cross sections. From further analysis, we find that the $\lambda = 3$ components of these transitions have a dominant contribution, whereas the $\lambda = 1$ components do not affect the 3^-_1 channel cross sections. In the present study, because of the lack of the experimental data, the $\lambda = 3$ strengths of the CL-A $\rightarrow 3^-_1$ transitions are assumed to be $B(E3) = 3.5$ W.u., as described in Sec. II B. To investigate the relation between the strengths of these transitions and the absolute value of the 3^-_1 channel cross sections, we make another assumption: The deformation lengths of the CL-A $\rightarrow 3^-_1$ transitions are assumed to be the same as the one that reproduces the $3^-_1 \rightarrow$ g.s. electric transition strength. The transition densities made with this deformation length may give transition strengths that are too strong for the cluster-shell transition, because both the ground and 3^-_1 states have a shell-model-like structure. We refer to these transition densities as *modified* transition densities, whereas those made in Sec. II B are referred to as *original* transition densities. In Fig. 5, the result of the full channel CC calculation using the modified transition densities (solid curve) is compared with the experimental data (solid circles). We also show the result using the original transition densities by the dashed curve, which is the same as the lowest solid curve in the left panel of Fig. 1. It is found that the solid curve well reproduces the angular distribution of the larger angles $\theta > 15^\circ$, although the cross sections at forward angles are less improved. This result indicates that the 3^-_1 channel cross sections at backward angles can be reproduced if the strengths of the CL-A $\rightarrow 3^-_1$ transitions are as strong as that of $3^-_1 \rightarrow$ g.s, but some unknown effects that are not considered in the present calculation will be necessary to reproduce the whole angular distribution.

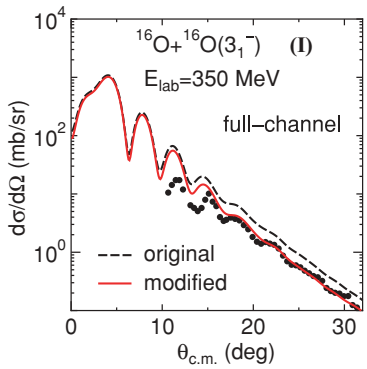

FIG. 5. (Color online) Angular distributions of the 3^-_1 channel at an incident energy of $E_{lab} = 350$ MeV by the full channel CC calculations using imaginary potential (I). The solid curve represents the result using the modified transition densities, whereas the dashed curve represents the result using the original transition densities (see text for details).

IV. SUMMARY

We have analyzed $^{16}\mathrm{O} + {}^{16}\mathrm{O}$ inelastic scattering to the $^{16}\mathrm{O} + {}^{16}\mathrm{O}$ $(2^+_1, 3^-_1)$ final channels at incident energies of $E_{lab} = 350$ and 1120 MeV by the microscopic coupled-channel calculation using the two types of imaginary potential (I) and (II).

We showed that the cross sections of the 2^+_1 channel can be well reproduced by our calculation without any artificial parameters, although the calculated cross sections slightly overestimate the experimental data only in the case of imaginary potential (I) for $E_{lab} = 1120$ MeV. We found that the rotational coupling among the 0^+_2, 2^+_1, and 4^+_1 channels plays a decisive role in reducing the cross sections of the 2^+_1 channel, despite the high incident energy $E_{lab} = 1120$ MeV ($E/A = 70$ MeV). This is because these three states have an $\alpha + {}^{12}\mathrm{C}_{g.s.}$ type cluster structure, and the strengths of the transitions $2^+_1 \rightarrow 0^+_2, 4^+_1$ are very strong owing to the large deformation. From this result, it can be said that the analysis of the nuclear reactions of unstable nuclei with a heavy ion target should be carefully done, because many molecule-type cluster structures are expected to exist in the ground and excited states in light unstable nuclei. However, the coupling effect with the other cluster channels (1^-_2, 3^-_2, 5^-_1, and 2^+_2) are found to be negligible. We also found that the coupling with the shell channels has a non-negligible effect on the 2^+_1 channel cross sections.

For inelastic scattering to the 3^-_1 channel at $E_{lab} =$ 350 MeV, we found that the cross sections are reduced by the coupling not only with the shell channels but also with the 0^+_2, 2^+_1, and 4^+_1 channels (referred to as CL-A), although the 3^-_1 state has a shell-model-like structure. However, the absolute values of the cross sections of this channel still overshoot the experimental data even by the full channel calculation. For the $E_{lab} = 1120$ MeV case, the coupling effect is very weak in (I) and is negligible in (II).

We further investigated the relation between the CL-A $\rightarrow 3^-_1$ transition strengths and the 3^-_1 channel cross sections in the $E_{lab} = 350$ MeV case, because electric transition strengths of these transitions are not available experimentally. We found that if the strengths of the CL-A $\rightarrow 3^-_1$ transitions are comparable with that of $3^-_1 \rightarrow$ g.s., the absolute value of the 3^-_1 channel cross sections at backward angles can be reproduced by our calculation. However, these strengths may be unphysically strong given the structures of the 3^-_1 state and CL-A states. Therefore, combined with the fact that the cross sections at forward angles cannot be reproduced by this prescription, the puzzle of the 3^-_1 channel still remains an open question, and more experimental information is needed for ^{16}O.

ACKNOWLEDGMENTS

The authors would like to thank Prof. H. G. Bohlen and Prof. D. T. Khoa for providing numeral data of the experimental cross sections and Prof. S. Okabe for providing the diagonal and transition densities of ^{16}O calculated by the OCM. M.T. thanks Dr. N. Ohtsuka for helping with the data and is also thankful to Prof. H. Horiuchi, Prof. K. Ikeda, and Dr. T. Furumoto for valuable comments. The numerical calculations were carried out on the Altix3700 BX2 computer at Kyoto University's Yukawa Institute for Theoretical Physics.

[1] M. El-Azab Farid and G. R. Satchler, Nucl. Phys. **A438**, 525 (1985).
[2] D. T. Khoa, G. R. Satchler, and W. von Oertzen, Phys. Rev. C **56**, 954 (1997).
[3] D. T. Khoa *et al.*, Nucl. Phys. **A672**, 387 (2000).
[4] M. Katsuma, Y. Sakuragi, S. Okabe, and Y. Kondo, Prog. Theor. Phys. **107**, 377 (2002).
[5] D. T. Khoa *et al.*, Nucl. Phys. **A759**, 3 (2005).
[6] Y. Fujiwara, H. Horiuchi, K. Ikeda, M. Kamimura, K. Kato, Y. Suzuki, and E. Uegaki, Suppl. Prog. Theor. Phys. **68**, 29 (1980).
[7] H. Horiuchi and K. Ikeda, Prog. Theor. Phys. **40**, 277 (1968).
[8] S. Okabe, in *Tours Symposium on Nuclear Physics II*, edited by H. Utsunomiya *et al.* (World Scientific, Singapore, 1995), p. 112.
[9] NNDC data base, http://www.nndc.bnl.gov/.
[10] Y. Sakuragi, M. Yahiro, and M. Kamimura, Prog. Theor. Phys. Suppl. **89**, 136 (1986).